Discrete metal nanoparticles with plasmonic chirality

Guangchao Zheng[a,b], Jijun He[c], Vished Kumar[d], Shenli Wang[e], Isabel Pastoriza-Santos[f,g], Jorge Pérez-Juste[f,g]*, Luis M. Liz-Marzán[d,h,i]*, Kwok-Yin Wong[b]*

[a.] *State Key Laboratory of Chemical Biology and Drug Discovery, Department of Applied Biology and Chemical Technology, The Hong Kong Polytechnic University, Hunghom, Kowloon, Hong Kong (China) Email: kwok-yin.wong@polyu.edu.hk*

[b.] *School of Physics, Zhengzhou University, Zhengzhou, 450001, Henan, China*

[c.] *Institute of Physics, Ecole Polytechnique Federal de Lausanne, CH–1015, Lausanne, Switzerland*

[d.] *CIC biomaGUNE, Basque Research and Technology Alliance (BRTA) Paseo de Miramón 182, 20014 Donostia - San Sebastian, Spain. E-mail: llizmarzan@cicbiomagune.es*

[e.] *College of Food Science and Nutrition Engineering, China Agricultural University, No.17 Qinghua East Road, Haidian District, Beijing 100083, People's Republic of China*

[f.] *CINBIO, Universidade de Vigo, Departamento de Química Física, Campus Universitario As Lagoas, Marcosende, 36310 Vigo, Spain) Email: juste@uvigo.es*

[g.] *Galicia Sur Health Research Institute (IIS Galicia Sur), SERGAS-UVIGO, 36310 Vigo, Spain*

[h.] *Ikerbasque, Basque Foundation for Science, 48013 Bilbao, Spain*

[i.] *Centro de Investigación Biomédica en Red, Bioingeniería, Biomateriales y Nanomedicina, CIBER-BBN, Paseo de Miramón 182, 20014 Donostia-San Sebastián, Spain*

Abstract

Chirality is present in our lives at all lengths scales, from the shape of galaxies to the conformation of single molecules. From the geometrical point of view chiral object does not have mirror planes or inversion symmetry but have the same physical properties, except that they often have opposite optical activities. Particularly interesting are optical properties of metallic nanoparticles called plasmonics and the implications that chirality can offer, that is, the selective interaction with either left or right-handed circularly polarized light. In this tutorial review, we summarise recent developments in the synthesis of discrete nanoparticles with plasmonic chirality, by means of wet-chemistry methods. We also present theoretical models that have been proposed to explain the chiroptical plasmonic response. We aimed at selecting the most relevant approaches that have been developed to confer individual plasmonic nanoparticles with chiroptical

features, together with the most promising applications that have been proposed to date. We expect this tutorial review to be of interest to researchers from a wide variety of fields that can make use of chiral plasmonics at nanoparticle level such as chemical sensing, photocatalysis, photodynamic therapy, photothermal Effects.

Introduction

Chirality is present in our lives at all lengths scales, from the shape of galaxies to the conformation of single molecules. From the geometrical point of view chiral object does not have mirror planes or inversion symmetry but have the same physical properties, except that they often have opposite optical activities. As a peculiar example, the pods of green beans prefer to fold into chiral helical structures (Figure 1A). A chiral object will interact differently with left-handed and right-handed circular polarized light at the absorption energy of the chiral objects. Based on these premises, a CD spectrum is obtained from the differential absorption and employed to discern the conformational structure of a chiral object. Many biologically active molecules, such as amino acids, proteins or DNA, exhibit circular dichroism (CD) in the ultraviolet (UV) region of the electromagnetic spectrum. The electronic and vibrational excitations of their chiral secondary structures are responsible for the differential absorption observed when illuminated with right- and left-handed circularly polarized light. Nevertheless, natural molecules show often weak chiroptical response. On the other hand, noble metal nanoparticles (NPs) can support localized surface plasmon resonances (LSPRs), collective and coherent oscillations of their conduction electrons confined at the metal-dielectric interface, upon excitation with an electromagnetic radiation. This optical phenomenon allows the confinement and manipulation of electrons at the nanoscale. The excitation of LSPRs generates highly intense electromagnetic fields at the nanoparticle surface, which can strongly interact with molecules located nearby giving rise to a variety of new phenomena such as surface-enhanced Raman scattering (SERS), surface-enhanced infrared absorption (SEIRA), plasmon-enhanced luminescence, or plasmon-enhanced CD. Thus the combination of chiral molecules with weak CD response and achiral plasmonic nanomaterials can give rise to a hybrid nanostructure with enhanced and tailored chiroptical properties.

Chiral plasmonic nanostructures can be also created through the synthesis of particles with chiral morphology, or by assembling achiral plasmonic nanoparticles into chiral configurations, often mediated by chiral molecular

templates such as DNA,[1] proteins,[2] polymeric fibers[3] among others[4, 5] (selected examples are shown in Figure 1). Regardless of the methodology employed for their fabrication, chiral plasmonic nanostructures exhibit significantly larger optical activity than natural molecules do. Particularly interesting are the light-manipulating capabilities that chiral nanomaterials can offer as circular polarizers, in enantioselective-based sensing, enantiomeric separation, and photocatalytic or photothermal chirality.

Typically, chiral plasmonic nanostructures are synthesized through either nanofabrication techniques, such as photolithography, or the directed-assembly of achiral plasmonic NPs. Unfortunately, these approaches present significant drawbacks such as limitations toward large-scale production in top-down fabrication methods, the lack of control in the dimensions and monodispersity of the assemblies or the directed-assembly approach or in the subsequent manipulations toward applications.

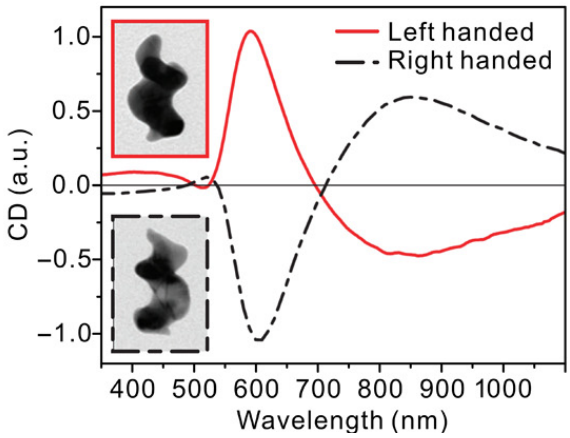
Left handed
Right handed
CD (a.u.)
1.0
0.5
0.0
−0.5
−1.0
400 500 600 700 800 900 1000
Wavelength (nm)

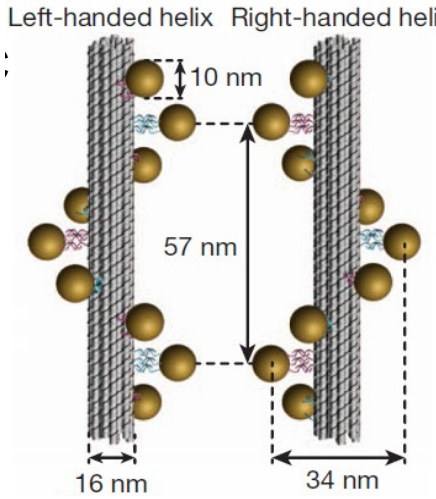
Left-handed helix
Right-handed helix
10 nm
57 nm
16 nm
34 nm

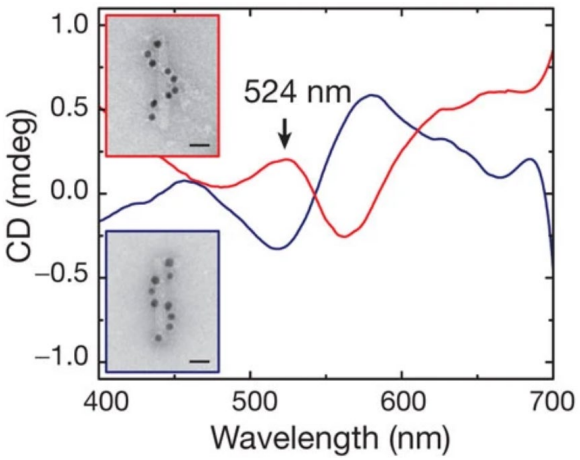
524 nm
CD (mdeg)
1.0
0.5
0.0
−0.5
−1.0
400 500 600 700
Wavelength (nm)

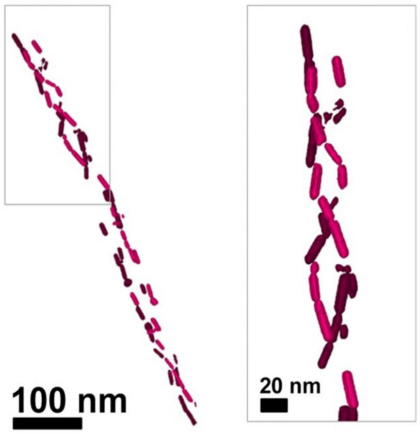
100 nm
20 nm

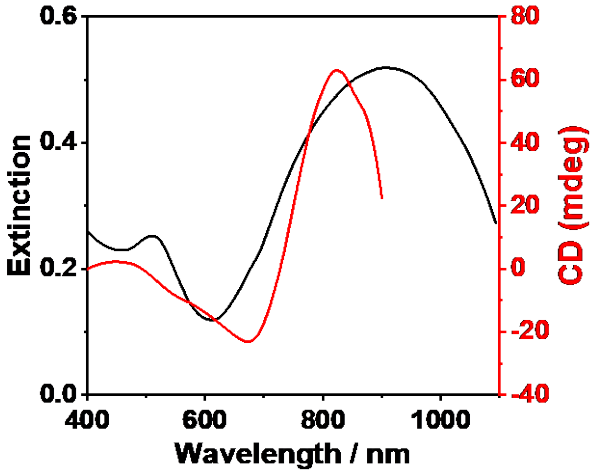
Extinction
CD (mdeg)
0.6
0.4
0.2
0.0
80
60
40
20
0
-20
-40
400 600 800 1000
Wavelength / nm

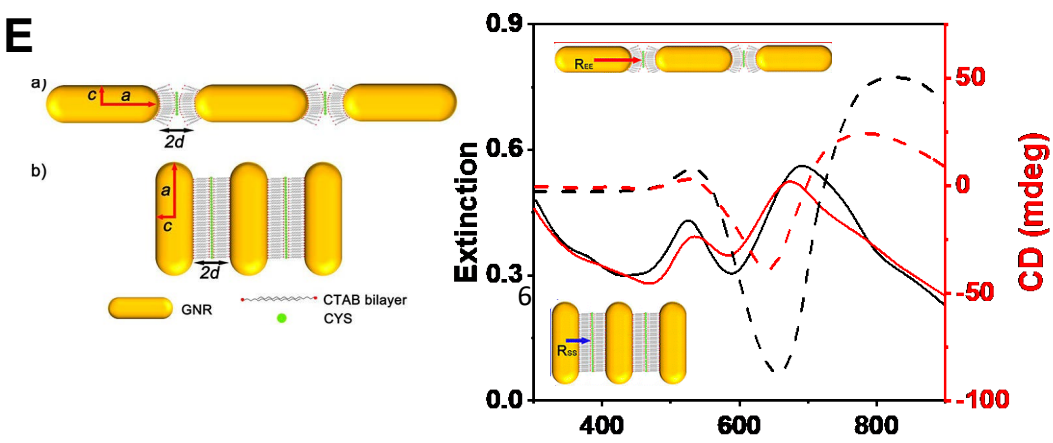
E
a)
b)
c
a
2d
GNR
CTAB bilayer
CYS
Extinction
CD (mdeg)
0.9
0.6
0.3
0.0
50
0
-50
-100
400 600 800

Figure 1. Examples of chiral (nano)structures. (A) Photograph of chiral pods of green beans grown from seeds. (B) TEM images and chiroptical response of Au nanohelices fabricated by nanolithography. The insets show representative TEM images of the helices. Adapted and reproduced from ref. [6]. Copyright 2013, Macmillan Publishers Ltd: Nature Materials. (C) Left: Scheme of nanohelices obtained *via* DNA origami-directed self-assembly of 10 nm Au nanoparticles. Right: Circular dichroism of left-handed (redline) and right-handed (blue line) nanohelices. The insets show representative TEM images. Adapted from ref. [7]. Copyright 2012, Macmillan Publishers Ltd: Nature (D) Left: Cryo-TEM tomography reconstruction of a 3D chiral arrangement of Au nanorods on an α-synuclein fibril and enlarged view of the top part of the assembly. Right: extinction and CD spectra of a colloidal dispersion of Au nanorod/α-synuclein self-assembled fibers. Adapted and reproduced from ref. [2]. Copyright 2018, National Academy of Sciences. (E) Left: Diagram of Au nanorods assembled in end-to-end, EE, (a) or side-to-side, SS, (b) structures, mediated by cysteine and CTAB. Right: Comparison of the optical properties of EE (black lines) and SS (red lines) assembled Au nanorods. Adapted and reproduced from ref. [8]. Copyright 2014, American Chemical Society.

Alternatively, these drawbacks can be circumvented by synthesising discrete plasmonic nanoparticles with dissymmetric morphology or through plasmonic nanoparticle-chiral molecule complexes. We present in this tutorial review the fundamentals of theoretical models that have been developed to understand the mechanism of plasmon-induced chirality, together with the most relevant methods for the synthesis of discrete chiral plasmonic nanoparticles and proposed strategies for their application in various fields. Although excellent reviews have been published regarding the fabrication, application, and theoretical understanding of chiral plasmonic nanostructures, most of them are devoted to nanostructures fabricated by molecular directed-assembly technologies.[9-12] Given the recent but fast development of the field, we decided to focus on wet-chemical approaches toward the synthesis of plasmonic nanoparticles with intrinsic chiroptical features, and their potential applications in the fields of enantioselective sensing and photocatalytic or photothermal chiral activity.

2. The origin of plasmonic chirality.

In general, a chiral object is defined as one which cannot be superimposed with its mirror image. In Chemistry, molecular chirality is commonly caused by a disymmetrical carbon atom, i.e. a carbon atom bonded to four different chemical groups or substituents. Notwithstanding, chirality and optical activity can also be found in a number of molecules which do not contain chiral carbon atoms. Examples include hexahelicene and ortho-condensed polycyclic aromatic compounds, which display a helical molecular structure giving rise to chirality and circular dichroism. These chiral molecules possess delocalized electron orbitals that extend over the entire structure. It should be noted that the optical activity of most chiral molecules is rather weak, due to their small extinction cross-section and/or low negative refractive index. Therefore, the applicability of CD spectroscopy to characterize the secondary structure (i.e., the types of molecular bonds), conformation and dynamics of biomolecules and macromolecules (i.e., the orientations of orbitals) requires either high concentrations or large volumes. In general, two main models have been proposed to demonstrate chiroptical activity in molecular systems, namely the helical model and the coupling of two mirror-symmetrically arranged electric dipoles.[13]

At the nanoscale, LSPRs in plasmonic nanoparticles enable the confinement of light and the generation of strong electromagnetic near fields, which might lead to enhanced molecule-metal chiroptical interactions. Numerous numerical and analytical theoretical models have been extensively developed to predict and understanding the optical properties of plasmonic nanostructures based on the resolution of Maxwell's equations.[14-16] Notwithstanding, plasmon-induced CD has been less studied and a complete understanding of this phenomenon would be necessary for an optimized development of efficient molecular-plasmonic systems. We provide herein a summary of state-of-the-art theoretical models to describe the plasmonic effect on the CD response of chiral molecules. Considering the size of plasmonic NPs, the effect of nanoplasmonics can be categorized as; *(a)* near-field induction model (dipole-dipole interactions) for nanoparticles with sizes much smaller than the wavelength of the incident light, i.e. $a_{metal} \ll \lambda$, and

(b) far-field induction model (electrodynamic interaction with retardation effect) for nanoparticles with $a_{metal} \sim \lambda$.[17]

The first model can be exemplified in a simple system comprising a chiral molecule and a spherical plasmonic NP, as shown in Figure 2A.[10, 18] In this molecule-NP complex, the chiral molecule is presented by electrical and magnetic dipole moments, $\boldsymbol{\mu}$ and **m,** respectively. The angle formed between $\boldsymbol{\mu}$ and **m** inside the chiral molecule can be influenced by the NP's LSPR, upon excitation with light.. Besides, the complex will show a new plasmon-induced CD peak at the LSPR wavelength produced by the chiral current generated inside the plasmonic NP *via* Coulomb dipole-dipole interaction.[18] Therefore, the chiroptical activity of chiral plasmonic nanostructures is determined by the nanoparticle size, the nature of the nanoparticle and the molecule, and the molecule-NP distance, R. When R is small, the Coulomb dipole-dipole interaction dominates the coupling between molecule and NP. Under this condition, the CD signal of the molecule-NP system (CD_{total}) can be described as a sum of two terms:

$$\mathrm{CD}_{\mathrm{total}} = \mathrm{CD}_{\mathrm{molecule}} + \mathrm{CD}_{\mathrm{plasmon}} \qquad (1)$$

where $CD_{molecule}$ and $CD_{plasmon}$ are the CD signal of the molecule and NP, respectively. $CD_{molecule}$ can be further expressed as:

$$\mathrm{CD}_{\mathrm{molecule}} = E_0^2 \frac{8}{3}\sqrt{\varepsilon_0 \omega_0} \frac{\Gamma_{12}}{|\hbar\omega - \hbar\omega_0 + i\Gamma_{12}|^2} \mathrm{Im}\left[\left(\widehat{P} \cdot \boldsymbol{\mu}_{12}\right) \cdot \boldsymbol{m}_{21}\right] = a(\omega) \cdot \mathrm{Im}\left[\left(\widehat{P} \cdot \boldsymbol{\mu}_{12}\right) \cdot \boldsymbol{m}_{21}\right] \quad (2)$$

where E_0 is the electric field of the incident light, ε_0 is the dielectric constant of the medium, ω_0 is the frequency of the molecular absorption, Γ_{12} is the broadening of the molecular transition from the ground state to the excite state, and $\widehat{P}$ is a tensor describing the plasmon-enhanced factor of the electrical field.[18, 19] The overall coefficient $a(\omega)$ indicates the absorption transition profile of the chiral molecule from the ground state $|1\rangle$ to the excited state $|2\rangle$. The equation clearly indicates that the chiral response of the molecule becomes larger as the plasmon-enhancement effect increases. This term reflects the plasmon-enhancement effect on the transition of the chiral molecule, which produces a

strong CD signal over the wavelength range of the molecule transition, see Figure 2B.[19]

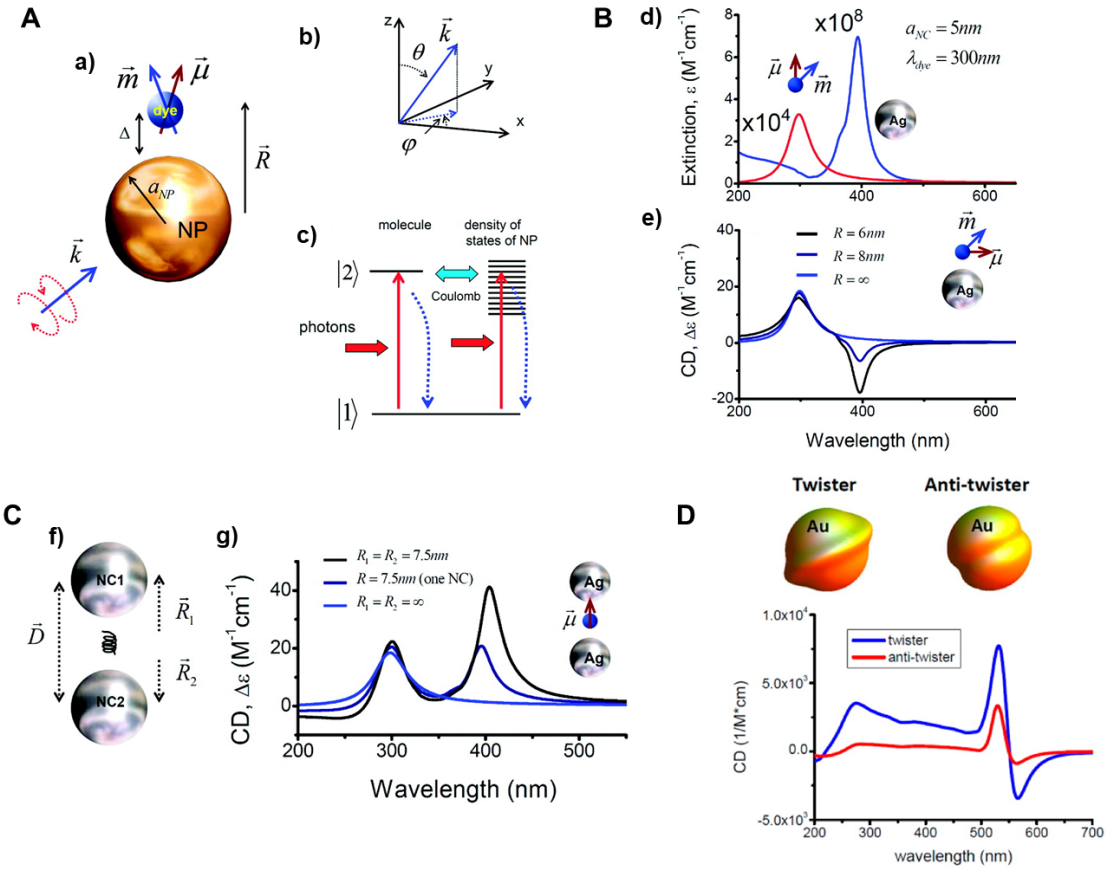

Figure 2. (A) Scheme of a complex composed of a metal nanoparticle and dye molecule (a). $\vec{R}$ denotes the vector connecting the centers of nanoparticle and molecule. (b) System of coordinates and the definition of polar angles used in the formulation. (c) Quantum transitions in the system; the solid vertical (horizontal) arrows represent light (Coulomb)-induced transitions. The dotted vertical arrows are the relaxation processes. Reproduced from ref. [18]. Copyright 2010, American Chemical Society. (B) Complex composed of an Ag NP and a dye molecule. (d) Extinction spectra of a molecule alone and a Au NP and (e) Calculated CD spectra for the Ag NP-molecule complex with three molecule-NP distance, R, as indicated. Reproduced from ref. [19]. Copyright 2011, American Chemical Society. (C) Model of a system composed of a NP dimer and a chiral molecule (f). (e) Calculated CD spectra of the dimer-molecule complex for two cases: $R_1 = R_2 = 7.5$ nm and $R_1 = R_2 = \infty$, being R_1 and R_2 the molecule-NP distance . The calculated CD spectrum for a single NP for R = 7.5 nm is also shown. Reproduced from ref. [19]. Copyright 2011, American Chemical Society. (D) Scheme of a right-handed twister and a antitwister Au NP with an average radius (R_0) of 7 nm and amplitude of variation of radius

(δR) of 1.5 and −0.8, respectively, together with the calculated CD response of both chiral Au NPs. Reproduced from ref. [20]. Copyright 2012, American Chemical Society.

The second contribution term of the CD signal in eq. 1 is the plasmon-induced CD, which is associated with the dissipation of light inside the plasmonic component. Considering a simple molecular-plasmonic system with spherical geometry,[17, 21] the plasmon-induced CD can be described as

$$\mathrm{CD}_{\mathrm{plasmon}} = \mathrm{Im}(\varepsilon_{\mathrm{metal}})\frac{8}{9}\frac{r_{\mathrm{metal}}^3}{\varepsilon_0 R^3}E_0^2\sqrt{\varepsilon_0}\left|\frac{3\varepsilon_0}{(2\varepsilon_0+\varepsilon_{\mathrm{metal}})}\right|^2 \mathrm{Im}\left[\frac{(\mu_{12x}\cdot m_{21x}+\mu_{12y}\cdot m_{21y}+\mu_{12y}\cdot m_{21x})}{\hbar\omega-\hbar\omega_0+i\Gamma_{12}}\right] \quad (3)$$

where $\varepsilon_{\mathrm{metal}}$ and r_{metal} are the dielectric function and radius of the plasmonic nanoparticle, *R* is the gap distance between the molecule and the plasmonic nanoparticles. $\mathrm{CD}_{\mathrm{plasmon}}$ is proportional to $\mathrm{Im}(\varepsilon_{\mathrm{metal}})$ given that absorption at the plasmon resonance takes place in the metal NP. In more complex molecular-plasmonic systems, it becomes more difficult to address the analytical expression of the plasmon-induced CD term. However, after taking reasonable approximations, it is possible to estimate the $\mathrm{CD}_{\mathrm{plasmon}}$ as follows

$$\mathrm{CD}_{\mathrm{plasmon}} \propto \mathrm{Im}(\varepsilon_{\mathrm{metal}})\cdot f_{\mathrm{resonant}}\cdot \mathrm{Im}\left[\left(\widehat{K}\cdot\boldsymbol{\mu}_{12}\right)\cdot\boldsymbol{m}_{21}\right] \quad (4)$$

where $\widehat{K}$ is an electromagnetic matrix describing the interactions between the molecular dipole and the plasmonic resonances, and f_{resonant} is a hybrid function describing the frequency-dependent plasmonic enhancement. $\mathrm{CD}_{\mathrm{plasmon}}$ will thus generate a CD signal at the plasmon resonance wavelength, which usually leads to a new peak in the CD spectrum (Figure 2B). [19]

Both contribution terms, $\mathrm{CD}_{\mathrm{molecule}}$ and $\mathrm{CD}_{\mathrm{plasmon}}$, show a positive correlation to the plasmon-induced enhancement of the electric dipole. This enhancement effect is proportional to R^{-3}, which means that it decreases rapidly as the molecule-NP distance increases. Therefore, obtaining an intense plasmon-enhanced CD signal would require that the chiral molecule be close to the surface of the plasmonic NP (Figure 2B).[22]

An alternative – though related – approach would involve placing the molecule within a plasmonic hotspot, i.e., a region of intense local field enhancement, usually at a small gap between two plasmonic nanostructuress. As an example, Figure 2C shows the case of a complex made of a nanoparticle dimer and a chiral molecule located at the gap between the NPs.[23] Theoretical calculations and experimental observations have consistently shown that, the electromagnetic near-field is much stronger at the interparticle gaps thereby leading to larger enhancements of the CD response. Such a hotspot-mediated plasmonic chirality can be artificially engineered, not only in intensity but also in position and handedness of the plasmonic CD peak.[8, 24-26]

When the size of the plasmonic NP is comparable to $\lambda/2$ of the incident light, the above-mentioned near-field induction model using the quasi-static approximation is no longer valid because of retardation effects.[27] In general, the constitutive relations of the molecule-plasmonic system can be defined as

$$\begin{cases} \mathbf{D} = \varepsilon\mathbf{E} + \xi\mathbf{H} \\ \mathbf{B} = -\xi\mathbf{E} + \mu\mathbf{H} \end{cases} \quad (5)$$

where D is the electric displacement field, E and H the electric and magnetic fields, B the magnetic induction and ε, ξ, and μ are parameters describing the properties of the chiral medium. ε, ξ, and μ are all 3×3 matrices due to the anisotropy of the chiral medium.[28] Furthermore, this equation can be written in several ways as

Tellegen's relations[29]
$$\begin{cases} \mathbf{D} = \varepsilon_0\varepsilon_\mathrm{r}\mathbf{E} + i\kappa\sqrt{\mu_0\varepsilon_0}\mathbf{H} \\ \mathbf{B} = -i\kappa\sqrt{\mu_0\varepsilon_0}\mathbf{E} + \mu_0\mu_\mathrm{r}\mathbf{H} \end{cases} \quad (6)$$

Post's relations[30]
$$\begin{cases} \mathbf{D} = \varepsilon_\mathrm{p}\mathbf{E} + i\xi_c\mathbf{B} \\ \mathbf{H} = i\xi_c\mathbf{E} + \mu_\mathrm{p}^{-1}\mathbf{B} \end{cases} \quad (7)$$

Drude-Born-Fedorov[31]
$$\begin{cases} \mathbf{D} = \varepsilon_\mathrm{DBF}(\mathbf{E} + i\chi\mathbf{B}) \\ \mathbf{B} = \mu_\mathrm{DBF}(\mathbf{H} - i\chi\mathbf{D}) \end{cases} \quad (8)$$

where ε_r, ε_p, and ε_DBF describe the permittivity of the medium, μ_r, μ_p, and μ_DBF describe the permeability of the medium and κ, ξ_c, and χ describe the chiral properties of the medium. In the case of a nonmagnetic medium (i.e. μ_p=1), taking Post's relations as an example, the constitutive parameters (ε_p and ξ_c) inside the formula can be derived as

$$\varepsilon_{\mathrm{p}}(\omega) = \varepsilon_c - \gamma_c \left(\frac{1}{\hbar\omega - \hbar\omega_0 + i\Gamma_{12}} - \frac{1}{\hbar\omega + \hbar\omega_0 + i\Gamma_{12}} \right) \quad (9)$$

$$\xi_c(\omega) = \beta_c \left(\frac{1}{\hbar\omega - \hbar\omega_0 + i\Gamma_{12}} + \frac{1}{\hbar\omega + \hbar\omega_0 + i\Gamma_{12}} \right) \quad (10)$$

where ε_c denotes the background refractive index, the coefficients γ_c and β_c determine the amplitude of absorptive and chiral properties. The coupling between the plasmonic NP and the chiral molecule can be considered by a far-field electromagnetic induction model. In this case, the properties of the plasmon-induced CD signal modification are generally investigated in molecule-plasmonic systems where the plasmonic NP is coated with layers of chiral molecules or embedded inside a chiral medium.

Besides generating enhanced CD via molecular-plasmon coupling, plasmonic nanostructures with an intrinsically chiral geometry can also provide strong CD signal.[2, 7, 20, 24, 27, 32] As an example, Figure 2D shows right-handed twister and a antitwister Au NPs exhibiting well-defined CD signals.[20] The total CD signal can be calculated through the absorption, Q,, of the chiral twisted plasmonic nanostructures, which can be expressed as

$$\mathrm{Q}_{\mathbf{k}} = \int \mathrm{d}V \langle \mathbf{j} \cdot \mathbf{E} \rangle_t = \mathrm{Im}(\varepsilon_{\mathrm{metal}}) \frac{\omega}{2\pi} \int \mathbf{E}_\omega \mathbf{E}_\omega^* \mathrm{d}V \quad (11)$$

k being the incident wavevector, ⟨...⟩t a standard time averaging and **j** the electrical current density. The integral represents the Joule heat generation in the whole volume of the plasmonic nanostructures. The directional CD for a certain wavevector **k** can then be defined as

$$\mathrm{CD}_{\mathbf{k}} = \mathrm{Q}_{\mathbf{k},+} - \mathrm{Q}_{\mathbf{k},-} \quad (12)$$

where $\mathrm{Q}_{\mathbf{k},+}$ *and* $\mathrm{Q}_{\mathbf{k},-}$ correspond to absorption for left- and right-handed circularly polarized light, respectively. Considering that the plasmonic nanostructures are randomly oriented in a colloidal system, the total CD signal is the integral of all orientations over θ_k and φ_k, i.e. the incident angles of the electromagnetic wave. For small nanostructures, the expresion of the total CD signal can be simplified by containing only the directional CD at three perpendicular directions:[33]

$$\mathrm{CD} = \langle \mathrm{CD}_{\mathbf{k}} \rangle_{\Omega_{\mathbf{k}}} = \frac{1}{4} \int \mathrm{CD}_{\mathbf{k}} \cdot \sin\theta_k \mathrm{d}\theta_k \mathrm{d}\varphi_k \approx$$

$$\frac{\mathrm{CD}_{\mathrm{k}\|+\mathrm{x}}+\mathrm{CD}_{\mathrm{k}\|-\mathrm{x}}+\mathrm{CD}_{\mathrm{k}\|+\mathrm{y}}+\mathrm{CD}_{\mathrm{k}\|-\mathrm{y}}+\mathrm{CD}_{\mathrm{k}\|+\mathrm{z}}+\mathrm{CD}_{\mathrm{k}\|-\mathrm{z}}}{6} = \frac{\mathrm{CD}_{\mathrm{k}\|+\mathrm{x}}+\mathrm{CD}_{\mathrm{k}\|+\mathrm{y}}+\mathrm{CD}_{\mathrm{k}\|+\mathrm{z}}}{3} \qquad (13)$$

In the above paragraphs, we summarized the theory of the CD properties of a molecule-plasmonic system. However, an analytical solution of the CD signal can only be obtained for a few systems under strict conditions (e.g., single chiral molecule and small metal nanosphere). In most cases, it is impossible to calculate directly the CD signal. Nowadays, various numerical methods have been developed which enable the design and optimization of chiral plasmonic systems, such as discrete-dipole approximation (DDA),[34] boundary element method (BEM),[16] surface integral equation combined with method-of-moments (SIE-MoM),[14] finite-difference time domain (FDTD),[35] and frequency-domain finite-element methods (FEMs).[36] These approaches have become popular, since they have been implemented in standard commercial software packages, such as COMSOL Multiphysics or Lumerical.[29, 31, 37-39]

The determination of the CD response of a certain chiral plasmonic system involves first the design of an appropriate model, which can be built by following different steps. First, the geometry of the plasmonic system is imported into the software, based on information obtained from electron microscopy analysis, and the electromagnetic fields are modified according to the selected constitutive relations. Second, the properties of the chiral medium (e.g. Eqs. 9 and 10) and plasmonic materials (e.g. using a Drude-Lorentz dispersion model) are directly written into the numerical model. Appropriate boundary condition and mesh are then selected.[20, 38] Finally, the absorption responses of the model under different incident light (i.e., LCP and RCP) and the corresponding CD signals are calculated using a numerical method.[40] The chiroptical activity of the chiral plasmonic complex nanostructures mainly results from their intrinsic chiral permittivity or/and chiral structures, which exist in several cases: (i) chiral molecules/templates adsorbed on plasmonic NP surface; (ii) chiral array of plasmonic NPs built by chiral molecules; (iii) nanomaterials with a chiral template shell or chiral twisted morphology. In summary, when plasmonic NPs meet with

chiral molecules/templates, or display helical chiral structures, a significant chiroptical activity can be achieved.

3. Synthesis of discrete chiral plasmonic NPs via wet chemical methods

Recent progress in wet chemistry has allowed the development of different routes for the synthesis of chiral plasmonic NPs. Those sinthetic routes can be classified into two main strategies: the Metal-Molecule-Metal (3M) and 3D chiral NPs. Scheme 1 summarizes both strategies, which are based on seed-mediated methods since they comprise as a first step the synthesis of nanoparticle seeds with well-defined shape and crystallography, subsequently followed by growth on the preformed NP seeds during which chirality is imparted. In 3M NPs (see Scheme 1), the final nanostructure involves a metal-molecule-metal core-shell-shell configuration, in such a way that chiral molecules constitute the inner shell and/or are embedded in the outer metal shell. The coupling of chiral dipoles from the molecule with the electromagnetic near-field generated at the inner hot-spots will be responsible for the chiroptical response. On the other hand, 3D chiral NPs show a chiral morphology (are dissymmetric), which is built up during the growth step, typically induced by chiral molecules present in the growth reaction medium.

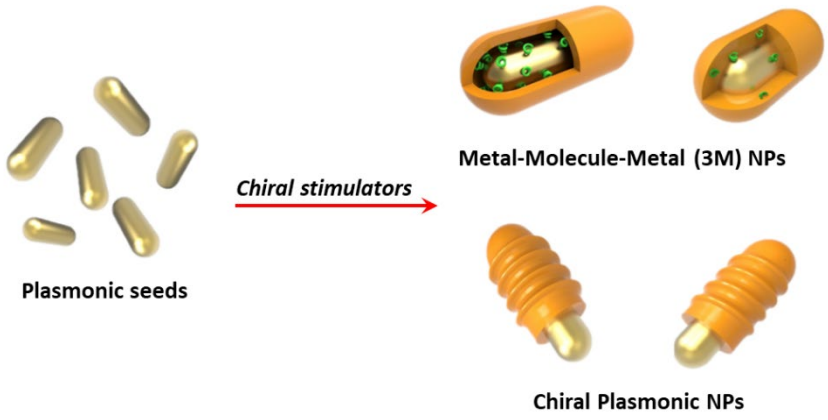

Scheme 1. Schematic representation of the two main strategies for the synthesis of chiral plasmonic nanoparticles, based on the seeded-growth of pre-synthesized plasmonic seeds: Metal-Molecule-Metal (3M) NPs and Chiral Plasmonic NPs.

Metal-Molecule-Metal (3M) nanoparticles. In what follows, we discuss the most relevant approaches so far to synthesize discrete chiral plasmonic NPs. We start with 3M NPs, which usually contain chiral molecules inside nanogaps or nanocavities present between the metal core and the outer metal shell of the NP. Such chiral molecules should thus contain suitable functional groups to promote binding onto the seeds surface and subsequent trapping during overgrowth of the outer metal shell. Different chiral biomolecules, such as peptides or DNA, which contain thiol and amine functional groups with strong binding affinity towards metal surfaces, have been used. The way chiral molecules adsorb onto the surface of the seeds, and therefore their surface distribution, are determined by parameters such as the crystalline structure and morphology of the metal seed, the concentration of chiral molecules, the bonding strength, etc.

Among the wide variety of available Au NP morphologies, Au nanorods (NRs) are arguably the most commonly used. The one-directional anisotropy of the rod-like morphology leads to straightforward tunability of the so-called longitudinal LSPR, thereby offering interesting prospects. Single crystalline NRs have been studied in particular detail and can be readily synthesized within a wide range of sizes and aspect ratios, thereby being perfect candidates as seeds to explore the influence of chiral molecule concentration on the morphology and chiroptical properties of the resulting 3M NPs.[40, 41] Zheng *et al.* investigated the influence of cysteine (Cys) concentration on the overgrowth of Au NRs (Figure 3A).[40] The results showed a conformal growth at low Cys concentrations (4 nM), the appearance of one or two spikes at medium Cys concentration (0.04 μM), and multiple spikes at high concentrations (0.4 μM). This Cys concentration-dependent growth was explained in terms of a surface blocking effect produced by the thiol group contained in the amino acid. Analysis of the chiroptical properties revealed that all overgrown Au NRs displayed bisignated plasmonic CD bands. Interestingly, those particles synthesized at medium Cys concentrations presented an anisotropy g factor apparently related to the transverse LSPR of 0.021, but also a plasmonic CD response associated with the longitudinal LSPR. Such a relatively high g factor was attributed to efficient Cys encapsulation and intense hot spots

generated at gaps between the Au core and the relatively thick outer Au shell, which enhanced the coupling of chiral dipoles with the electromagnetic near field. Moreover, the plasmonic CD bands of 3M Au NPs can be red-shifted by further coating them with silica, due to the increase in the dielectric permittivity of the sourrodunding medium (Figure 3A).

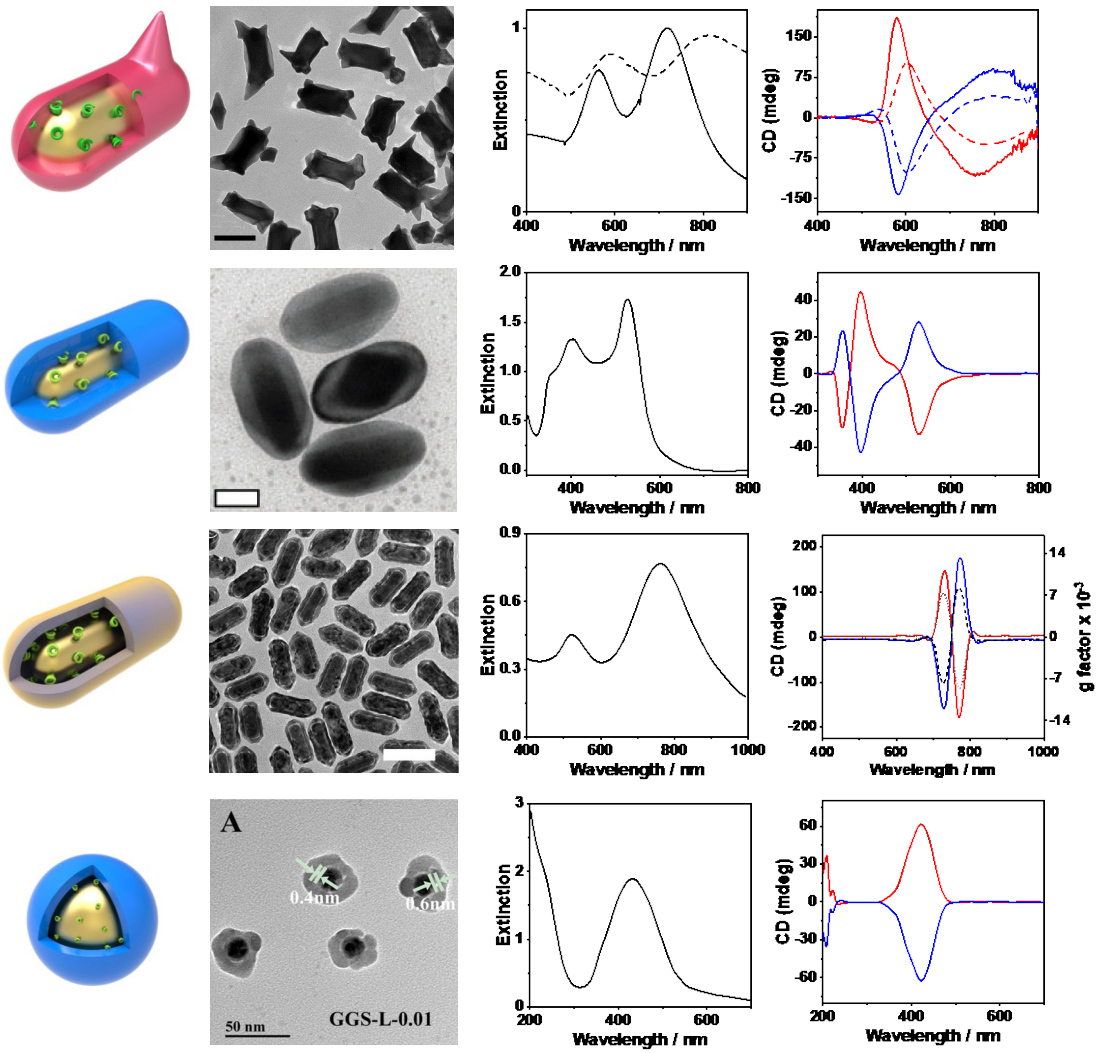

Figure 3. Schematic representation of different 3M chiral NPs, together with representative TEM images and corresponding extinction and CD spectra. (A) Au@Au core-shell nanorods (Scale bar: 100 nm). The dashed lines correspond with the after the silica coating showing a red-shift in both, the extcntion and CD spectra. Reproduced from ref. [40] Copyright 2018, Wiley. (B) Au@Ag core-shell nanorods (Scale bar: 20 nm). Reproduced from ref. [42]. Copyright 2016, Royal Society of Chemistry. (C) Au@AgAu yolk-shell nanorods (Scale bar: 100 nm).

Reproduced from ref. [43]. Copyright 2018, Wiley. (D) Au@Ag core-shell spheres. Reproduced from ref. [44]. Copyright 2015, Wiley.

Similar results were reported for both Cys and penicillamine-modified Au NRs, upon overgrowth with Ag (Figure 3B).[42] The entrapment of amino acids within the Au-Ag interface and the corresponding amplification of the electromagnetic near field were found to induce a moderate enhancement of the plasmonic CD response (g factor of 0.0013). The chiroptical response of Au@Ag NRs was further improved by transforming the Ag shell into an AgAu yolk-shell NR structure via galvanic replacement, which allowed to further engineer the interior nanogap and achieve a higher g factor of 0.009 (Figure 3C).[43]

A similar strategy has been demonstrated for core-shell nanospheres with an interior nanogap fabricated with cysteine enantiomers that confer them with plasmon-induced circular dichroism properties (Figure 3D).[44, 45] The interior nanogap of Au@Ag sphere could be manipulated by varying cysteine concentration, and anisotropic g-factors as high as 0.01 were reported. Alternatively, plasmon CD signals could be generated in Au@Ag nanospheres by using cytosine-rich single stranded DNA as the template to guide silver shell growth. The DNA-plasmon interaction could be further amplified by electromagnetic coupling of the core-shell structure as the Ag shell thickness was increased, with a highest anisotropic factor reported for a spherical NP of 0.0193. Unlike chiral NRs, the chiroptical response of spherical nanostructures does not offer a wide range of tunability.

3D chiral nanoparticles. The construction of NPs with intrinsic chiral morphology in 3D (3D chiral NPs) is more conceptually challenging, since it involves drastic changes in the way metal atoms are deposited on the (achiral) seed NP. As a result, the development of this approach has been slower and we can distinguish two main approaches among the few existing reports. The common concept between both strategies is the use of chiral molecules (such as peptides, aminoacids and surfactants) to try dictate the seeded-growth of pre-formed NPs, confering them with chiral morphological features. Arguably, the most impressive

results so far were obtained by Nam and co-workers, who reported the synthesis of so-called “plasmonic helicoids”, with intricate twisted morphologies deriving from either cubic or octahedral NP seeds, using enantiomers of cysteine and glutathione as chirality inducers.[46] Indeed, the origin of chirality in the final NPs was attributed to an enantioselective interaction between the chiral molecules and chiral components at the NP surface, such as high miller index surfaces or kink sites. Chiral NPs were obtained by a seeded-growth process, typically using 50 nm cube-shaped gold seeds with low-index (100) planes, which were overgrown in the presence of chiral molecules, into NPs with high Miller index surfaces . The interaction of certain functional groups (thiol, amine, carboxylic, etc.) in the chiral molecules with the Au surface was proposed to play a critical role in controlling NP growth. Using this strategy, different helicoids with tailored handedness and strong chiral plasmonic resonances were fabricated.

It should be noted that, in the absence of chiral amino acids, the overgrowth of gold nanocubes resulted in the formation of symmetric and achiral stellated octahedra with 48 identical {321}[47] triangular facets in alternating R (clockwise) and S (anti-clockwise) conformation, which can be defined by the rotational direction of low-index planes (100), (110), and (111) (Figure 4). Oppositely, the presence of L-Cys or D-Cys enhanced the growth of right-handed or left-handed chiral nanostructures, as a result of different growth rates at the two oppositely chiral high-index planes of gold nanoparticles. Cysteine enantio-selectively interacts with {321} high index surfaces at stellated octahedra, resulting in the splitting and growth of the boundaries between $\{321\}^R$ and $\{231\}^S$ of R and S regions in the [101] direction, causing the symmetry of the stellated octahedron to change from the 4/m32/m point-group symmetry into 432 symmetry. Thus, when L-cysteine was used, R-S boundaries tilted by an angle -ø towards the S region, whereas with D-cysteine it tilted towards the R region by +ø. This preferential growth was attributed to a different the binding affinity of R and S kink sites with a specific cysteine enantiomer, hindering the vertical growth of that particular plane with respect to the other, and thereby causing the boundary to shift towards the plane with faster growth. Further, asymmetric growth along the (100) and (111) directions resulted in protruded vertices with split and twisted edges, creating a nm-scale gap inside these

helicoids (Figure 4C). These chiral NPs, referred to as 432 Helicoid I, featured a dissymmetry factor of 0.03. By using glutathione molecules instead of cysteine in the growth solution, an overgrowth of the boundaries between $\{321\}^R$ and $\{312\}^S$ facets in the 011 direction was obtained. Although seeded growth occurred through the same intermediate nanostructure as that for 432 Helicoid I, the use of the larger glutathione molecule changed the interaction with the metal surface, giving rise to a different chiral nanostructure with pin wheel-like features and four-fold symmetry along the 100 direction (Figure 4D). These chiral NPs (432 Helicoid II) had a higher dissymmetry factor of 0.05. Yet a different type of chiral nanostructure was obtained by using octahedral Au seeds enclosed by eight (111) facets, in the presence of glutathione. The morphological evolution involved rhombic dodecahedral intermediates and eventually led to a pin wheel-like structure with more twisted features, and deeper gaps running radially from the center. A remarkable dissymmetry factor to 0.20 was recorded for these 432 Helicoid III NPs (Figure 4E), which is a large increase with respect to 432 Helicoids I and II. In a subsequent improvement of the morphological homogeneity, the chiroptical response of these helicoid nanoparticles could be further enhaced up to 0.31. Such an optimization involved a multi-chirality-evolution synthesis with precise control over the growth kinetics in a sequential growth process.[48]

The most recent studies from Nam's group focused on improving the chiral optical response of helicoid NPs. [49] By carefully analysing the effect of various parameters, such as peptide sequence, seed morphology, or concentration of reactants, on the growth kinetics and the chiral features of the resulting NPs, both particles with improved chiroptical response and new helicoidal shapes could be obtained.

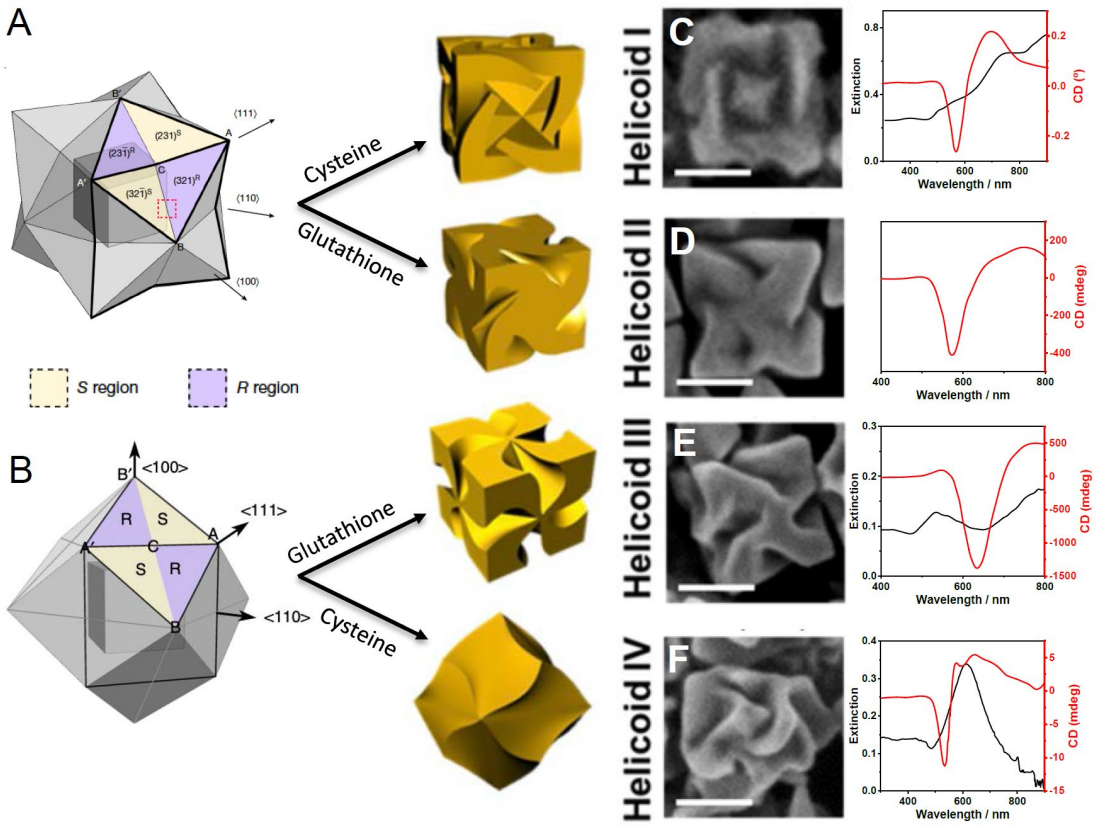

Figure 4. (A-B): Schematic representation of a stellated octahedron (A) and rhombic dodecahedron (B), differentiated by high-index facets consisting of S region and R region configurations and the respective evolution of these nanostructures into different helicoids. (C-F) SEM images and corresponding CD spectra of: 432 Helicoid I (C), 432 Helicoid II (D), 432 Helicoid III (E), and 432 Helicoid IV (F). Adapted from refs. [46]. Copyright 2018, Macmillan Publishers Ltd: Nature. Ref. [49]. Copyright 2020, Macmillan Publishers Ltd: Nature Communications. Ref. [48]. Copyright 2020, American Chemical Society.

A conceptually different approach involving the use of chiral co-surfactants to template the growth of Au nanorods with screw-like helical features, was recently demonstrated by Liz-Marzan and co-workers. In this process, strong binding of chiral molecules is not required to direct dissymmetric growth. On the contrary, chiral co-surfactants such as 1,1'-bi(2-naphthol) (also known as BINOL) and 1,1'-binaphthyl-2,2'-diamine (BINAMINE) were used in combination with a quaternary ammonium surfactant (CTAC) to obtain chiroptically active, worm-like micelles, which adsorb on pre-formed Au NRs in a quasi-helical pattern, subsequently acting as templates to guide seeded-growth. As a result, pronounced wrinkles were produced, which handedness was determined by the specific

co-surfactant enantiomer used during growth. The chiral features on the overgrown NRs were significantly better defined when BINAMINE was used, which is likely related to the presence of two amine moieties in chelating configuration, with a higher affinity to the Au surface in comparison to the hydroxy groups in BINOL. High quality electron tomography reconstructions of chiral nanocrystals obtained using (R)-BINAMINE confirmed the presence of sharp wrinkles grown quasiradially, with tilt angles ranging from 0˚ to 45˚ with respect to the short AuNR axis, as well as an ill-defined structure when using (R)-BINOL (Figure 5A-D). A detailed analysis of orthoslices through the 3D reconstructions revealed an intricate network of wrinkles of varying heights, but with consistent width and inter-groove distances. Through 3D fast Fourier transformation, it was possible to identify the areas that contribute most to the chirality of the structure (Figure 5E). A correlation was observed, not only between the handedness of the helical structure with the enantiomeric form of the co-surfactant, but also between the size of micelles in solution and the measured interwrinkle distances on the NR surface. It was therefore suggested that the templating mechanism involves the micelles acting as patterns that direct the diffusion and surface-reduction of gold ions (likely complexed to CTA^+ molecules). The formation of sharp wrinkles is thus driven by a fast deposition rate of gold ions at available sites between CTAC/BINAMINE micelles on the NR surface. The extent of the wrinkles could be adjusted through the ratio between Au NR seeds and the reagents in the growth solution, leading to overall sizes ranging from 165x73nm to 270x175nm. A most interesting observation was the possibility to tune the plasmonic CD bands, from 700 nm up to 1600 nm, by varying the dimensions of the wrinkles on Au NRs. As-synthesized chiral nanocrystals exhibited high dissymmetry factors in the visible (~0.20), and estimated values close to 0.30 in the near IR (Figure 5F,G). Broad applicability of this method was demonstrated by overgrowing Pt grooves over Au NRs (Figure 5H-I), as well as using spherical AuNPs as seeds (Figure 5J).

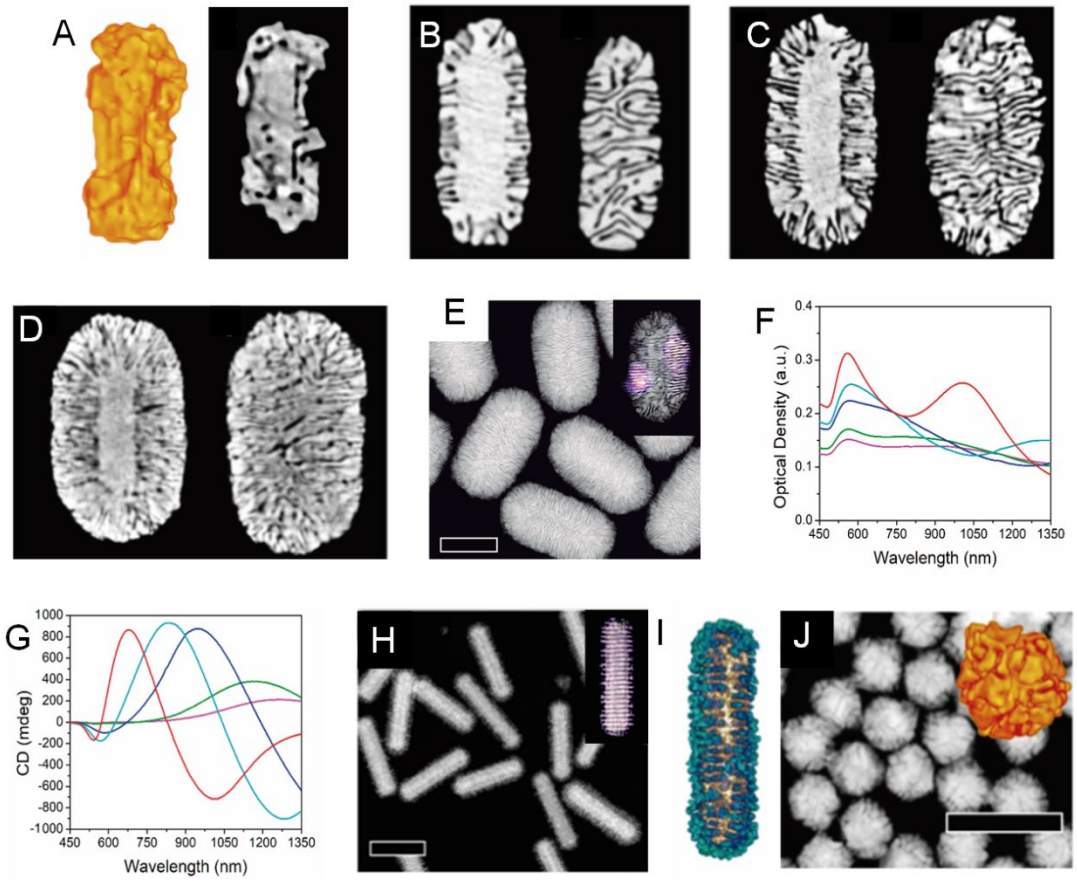

Figure 5. Chiral nanorods templated by helical surfactant micelles. (A) Tomography reconstruction of a gold nanorod overgrown in the presence of (R)-BINOL (left) and a selected orthoslice (right). (B-D) Orthoslices through 3D reconstructions from different chiral nanorods synthesized in the presence of (R)-BINAMINE, with sizes 165x73nm (B), 210x112nm (C), 270x175nm (D), revealing the presence of the central NR (left) and a radial wrinkle network (right). (E) HAADF-STEM Image of chiral 210x112nm nanorods (scale bar: 100 nm) and an exemplary inverse FFT showing the areas of particle with chiral features, indicating right handedness (inset). (F,G) Vis-NIR (F) and CD (G) spectra of chiral nanorods with varying particle dimensions: 165x73nm (red), 200x92nm (cyan), 250x145nm (green), 270x175nm (magenta). (H) HAADF STEM Image of Au@Pt wrinkled nanorods (scale bar: 100 nm) and inverse FFT (inset). (I) Tomography reconstruction of Au@Pt nanorods in EDX mode, showing the pattern of Pt grooves (cyan) on the central Au NR (golden); (J) HAADF-STEM Image of chiral nanospheres and a 3D reconstruction (inset). Reproduced from ref. [50]. Copyright 2020, American Association for the Advancement of Science (AAAS).

Other approaches. Other plasmonic nanostructures with chiroptical properties have been reported, based on the use of soft and hard templates. For instance,

Nakagawa and Kawai obtained double-helical Au nanowires with moderate optical activity, by using twisted nanoribbon soft templates obtained by mixing D- or L-12-hydroxystearic acid (HSA), which transfer their conformation to the nanowire helical nanostructures, and a long chain amidoamine (C18AA) serving as capping agent for Au.[51] In another approach, inorganic nanostructures with chiral shape were also proposed as hard templates to obtain chiral plasmonic nanostructures. Markovich and co-workers reported the synthesis of colloidal Te nanostructures with both chiral lattice and chiral shape resembling a trigonal prism with twisted ridges,[52] using strongly binding chiral ligands and showing a large peak dissymmetry within the visible. Subsequently, chiral tellurium nanostructures were transformed into chiral gold nanostructures through galvanic replacement, resulting in a meaningful chiroptical activity (g-factor 0.003). Another interesting approach made use of circularly polarized light as the source of chirality to be transferred onto the plasmonic nanostructures. Tatsuma and co-workers reported the fabrication of chiral plasmonic nanoparticles by selective deposition of a dielectric material such as PbO_2 on the surface of achiral Au nanocuboids, taking advantage of plasmon-induced charge separation that occurs when the particle is in contact with a semiconductor.[53] Depending on the handedness of the incident circularly polarized light, the localized electric field distributions around the achiral nanocuboids are twisted and localized at different corners driven the selective deposition of PbO_2 by Pb^{2+} oxidation. Furthermore, the handedness of the chiral plasmonic nanostructure can be reversibly switched between right and left by a reduction-oxidation process of PbO_2 under UV and circularly polarized light, respectively.[54]

4. Applications of discrete chiral plasmonic NPs

We focus in this section on promising applications for discrete chiral NPs, largely in the fields of chemical sensing, circularly polarized photocatalysis, photodynamic therapy, among others. Among the different applications described we also consider those initially developed with chiral NPs fabricated through physical methods due to their exceptional chiroptical performance.

Chemical sensing. Label-free LSPR sensors rely on the high sensitivity of plasmonic nanostructures toward changes in the refractive index of their local surrounding medium. Any change in the nanostructures environment, for instance related to molecular binding, can be readily tracked by an LSPR shift.[55, 56] LSPR-based sensors have demonstrated a relatively high sensitivity and speed, as well as simple-to-operate detection, and are therefore considered as effecient chemical sensors, even though they usually feature modest figures of merit (FOMs). Chiral plasmonic nanoparticles offer an attractive alternative, since they are characterized by rich CD spectral features with bipolar nature and multiple zero-crossing points, thereby maximising LSPR sensitivity and FOM (Figure 6A-D). Jeong *et al.* developed an analytical model for chiral plasmonic sensing that clearly shows the importance of chirality and material properties in the sensing performance.[57] Considering that the FOM is defined as the relationship between the refractive index sensitivity and the accuracy (standardised as the full width at half maximum, FWHM), the following expression can be derived:

$$\mathrm{FOM} = {2\bar{\chi}|\delta\chi|\mathrm{n}^3}\Big/{\varepsilon_i^2\sigma}$$

Where $\bar{\chi}$ is an achiral term, $\delta\chi$ a chiral shape factor specific to right or left handed enantiomers, n is the refractive index of the local medium, ε_i is the imaginary part of the dielectric constant and σ the instrument resolution.

This equation clearly indicates that the chiral shape factor, $\delta\chi$, is decisive in the FOM. An increase in $\delta\chi$ gives rise to a larger FOM. Considering this rule, the same authors used a physical vapour deposition technique to fabricate alloyed Ag-Ti nanohelices where the chiroptical properties could be tuned by adjusting the chiral shape factor and dielectric function of the nanoparticles by varying the Ag and Ti content. Interestingly, the sensitivity of these nanohelices could be improved by increasing either their length (which increases the chiral shape factor), or the percentage of Ti in the alloy (flattering the dielectric function). As a result, these hybrid nanohelices could exhibit sensitivities of ~1,100 nm per refractive index unit (RIU) with a FOM of ~2,900 RIU^{-1}, which are large values

considering those previously reported for LSPR sensors.[57] As a proof of concept, the specific detection of biotin-avidin interaction was demonstrated.

Chiral nanostructures based on the assembly of chiral plasmonic nanoparticles have been demonstrated to perform particularly well in chemical sensing. The key concept is that the interparticle coupling (or hybridization) of chiral plasmon modes results in enhanced chiroptical activity and its corresponding sensitivity. For instance, Xu *et al.* proposed 3M Au@AgAu chiral NRs and Au nanospheres, as building blocks for chiral core-satellite assemblies mediated by DNA hybridization of complementary strands on each component.[43] These chiral nanostructures display much stronger plasmonic CD intensity and larger g-factors than the individual building blocks (0.021 *vs* 0.009, respectively), likely due to a cooperative chirality combining the structural chirality of the nanorods and plasmon-induced molecular chirality. Interestingly, chiral plasmonic core-satellite nanostructures fabricated using a Zn^{2+}-specific DNA-cleaving DNAzyme were applied to quantitatively detect zinc ions in living cell lines (primary uterine fibroblast cells and HeLa cells). In the presence of the target Zn^{2+}, the DNAzyme strand catalyses the cleavage of the complementary DNA strand on the Au satellites inducing disassembly of the core-satellite structure. By monitoring the resulting decrease in CD response, Zn^{2+} concentration could be quantitatively determined (Figure 6E and F).

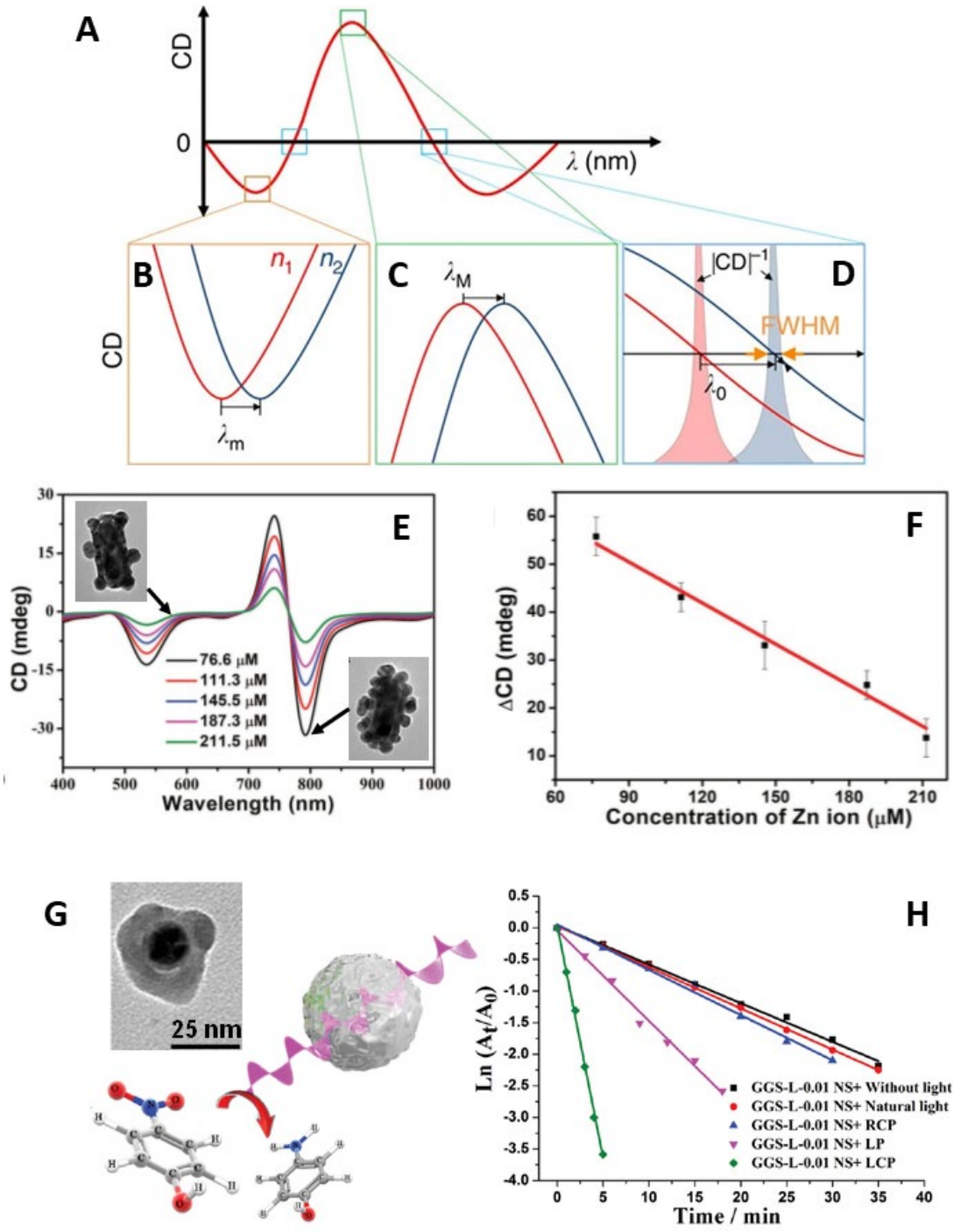

Figure 6. (A-D) Chiral plasmonic sensing. (A) CD spectrum of a plasmonic enantiomer as a function of wavelength. (B-D) Resonance shifts at the minimum λ_m (B), maximum λ_M (C) and half maximum λ_0 (D), where the refractive indices of the surrounding media are varied from n_1 to n_2. Reproduced with permission from ref. [57]. Copyright 2015 Nature publishing group. (E-F) CD spectral changes with different concentrations of intracellular Zn^{2+} (E) and calibration curves for Zn^{2+} detection (F), where $\Delta CD = CD_{740\ nm} - CD_{795\ nm}$. The insets in (E) show representative TEM images showing a decrease in the number of Au

satellites in the assembly with increasing concentration of Zn^{2+} ions. Reproduced with permission from ref. [43]. Copyright 2018, Wiley. (G-H) Schematic representation of the circularly polarized photocatalysis of 4-nitrophenol to 4-aminophenol by 3M Au@Ag chiral NPs (G). The inset shows a representative TEM image of a 3M Au@Ag chiral NP. (H) Kinetic trace (plot of Ln (A_t / A_0) as a function of time) for the reaction catalyzed by 3M Au@Ag chiral NPs under different light conditions (RC, L and LC stand for right-circularly, linear and left-circularly polarized light). Reproduced with permission from ref. [45]. Copyright 2015, Wiley.

Enantioselective chemical sensing is a field in which chiral plasmonic nanoparticles may play a particularly important role. Liu *et al.* recently proposed a chiral nanostructure consisting of a gold nanorod coated with a chiral mesoporous silica shell to semiquantitatively measure the composition of chiral enantiomers by means of SERS.[58] The growth of the chiral shell onto the Au NRs was directed by using amino acid derived chiral surfactants as the template molecules. The strong near-field coupling between Au NR and the chiral molecules on the shell confers the system with a strong chiroptical activity in the visible and NIR regions. By simply adding chiral cysteine molecules, they get infiltrated in the porous shell, as demonstrated by SERS spectroscopy. Interestingly, when cysteine molecules and the shell present the same handedness a new peak appears in the SERS spectrum, but this was not evident with cysteine and shell of opposite chirality. The difference in SERS spectra was ascribed, and demonstrated by theoretical calculations, to a conformational change of chiral cysteine molecules when they are docked inside the chiral mesoporous silica shells with the same handedness. Additionally, a semi-quantitative determination of the amount of cysteine enantiomers in solution was demonstrated, thereby becoming a promising platform for the sensitive SERS determination of enantiomeric ratios.

Circularly polarized photocatalysis. Plasmonic nanostructures exhibiting large chiroptical asymmetries are expected to generate plasmon-induced hot electrons, which is intimately related to near-field enhancement,[59] and therefore

will be dependent on the polarization of incident circularly polarized light. Fang and co-workers demonstrated dichroic hot electron transfer from chiral Au crescent-like nanoparticles to TiO_2, where differences in the incident photon-to-charge conversion efficiency (IPCE) between right and left-handed circularly polarized illumination were in agreement with standard CD extinction measurements.[60] Additionally, by using cathodoluminescence spectroscopy they were able to show that the chiral response is caused by the polarization dependence of the local field hot-spot distributions associated with the corresponding plasmon resonances. As a result, the circularly dichroic effect of asymmetric hot electrons could enhance different photochemical processes. On a related report, Xu *et al*. studied the effect of circularly polarized light on the catalytic performance of 3M Au@Ag chiral NPs towards the reduction of 4-nitrophenol (4-NP) into 4-aminophenol (4-AP), in the presence of borohydride. This reaction, which takes place at the surface of metal nanoparticles, is a well-known model to evaluate the catalytic activity of nanocatalysts and can be easily monitored by UV-Visible spectroscopy.[61] The results showed that, irradiation with circularly polarized light with the same handedness as the plasmonic nanoparticles gave rise to catalytic efficiencies at least 10-fold higher than the photocatalytic reaction with linearly polarized, natural light or in the absence of light (Figure 6G and 6H).[45] Such a catalytic performance was ascribed to the increased generation of hot electrons by chiral plasmonic nanoparticles when irradiated with light of matching circular polarization.

Circularly polarized photodynamic therapy. Photodynamic therapy combines light energy with a drug (photosensitizer), which is initially non-toxic but is designed to induce cell death (by reactive oxygen species (ROS) generation) upon activation by light. Plasmonic nanoparticles can readily display higher extinction coefficients than standard organic photosensitizers and can therefore be used to transfer energy to molecular oxygen with high efficiency and selectivity for the generation of singlet oxygen species ($^1O_2$). The efficacy strongly relies on the optical properties of plasmonic nanoparticles, since plasmons can delay the recombination rate of electrons and holes.[62] Therefore, chiral plasmonic nanoparticles should be able to act as photosensitizers under circularly polarized

light irradiation. For instance, Gao *et al.* proposed DNA-driven core-satellite Au assemblies as chiral photosensitizers.[63] These nanostructures, exhibiting chiroptical properties in the visible region, show highly efficient ROS generation at least three times higher than that provided by protoporphyrin IX, a standard organic photosensitizer. Illumination with either circularly polarized light with opposite handedness or linearly polarized light, did not induced ROS production, which was ascribed to insufficient energy transfer efficiency. The potential of such core-satellite Au assemblies as chiral photodynamic therapy agents was demonstrated both *in vitro* and *in vivo*.

Chiral Photothermal Effects. Upon LSPR excitation of a plasmonic nanoparticle with light, enhanced absorption and/or scattering processes occur at the NP surface. Both processes depend on the nature and the shape of the particles, the absorption scales linearly with volume, whereas scattering varies as volume squared. Plasmonic nanostructures can thus convert absorbed light into heat, and subsequently transfer this energy to the surrounding medium giving rise to a temperature increase.[64] This thermal dissipation (or lattice cooling) is responsible for well-known photothermal effects, which have been used for biomedical applications. Similarly, photothermal chirality originated from the differential absorption of circularly-polarized light by chiral plasmonic nanoparticles could also be exploited in various fields. Miandashti and coworkers experimentally demonstrated photothermal chirality originating from the differential absorption of circularly-polarized light by left-handed Au helicoids.[65] The photothermal response was measured by luminescence thermometry through spin-coating the chiral nanoparticles on a AlGaN:Er^{3+} thin film. Upon LSPR excitation, an increase in the temperature, attributed to the absorption cross section of the Au helicoids, was observed. A comparative study, performed between LCP and RCP illumination of spin-coated Au helicoids, showed a net increase in temperature of 6 °C when irradiated with RCP compared to LCP illumination. Additionally, an increase of the laser excitation intensity by 12 times generated a temperature increase as high as 50 K. Interestingly, since the temperature increase is directly proportional to both the absorption cross section and the laser intensity, optical

and photothermal effects should produce similar *g*-factors, i.e. if a chiroptical *g*-factor of 0.1 were observed a 10% higher temperature would be obtained for RCP light illumination.

Other applications. CD is mainly caused by molecular electron energy level transitions, due to differences in the refractive index and absorption coefficient of optical materials. Therefore, the characterization of enantiomers is usually carried out measuring CD spectra based on the extinction response to RCP or LCP light. Additional information may be obtained by analysing the vibrational modes under irradiation with RCP or LCP light. Thus, vibrational CD (VCD) and Raman optical activity (ROA) spectra are associated with molecular vibrational modes and carried out with near-infrared laser irradiation. Bearing this in mind, the chirality transfer from one molecule/nanostructure to another could also become important toward the development of new applications in chiral technology. Dolamic *et al*. showed that, an intrinsically chiral gold cluster can transfer its handedness to an achiral molecule, such as 2-phenylethylthiolate, adsorbed on its surface. [66] VCD spectra showed certain signals associated with the preferential adsorption of the molecules adopting a chiral conformation. In a different approach, Pour and coworkers demonstrated the chirality transfer from a chiral molecule (ribose or tryptophan) into an achiral plasmonic nanostructure comprising Ag@SiO_2 core-shell nanoparticles doped with a resonant Raman achiral dye (benzotriazole with an absorption maximum at 514 nm). Covalent surface modification of Ag@SiO_2 NPs with the chiral molecule induced a symmetry breaking of the LSPR, which becomes chiroptically active as demonstrated by the opposite mirror bands exhibited in the ROA spectra recorded for both enantiomers of the chiral molecule (Figure 7A). This is the first report of chirality transfer from a chiral molecule to an achiral one, mediated by a plasmonic nanoparticle. This approach could open a new route to study the conformation of molecules near a plasmonic surface for enantiomer recognition.

Plasmonic nanostructures with large *g*-factor can selectively absorb circularly polarized light with the same handedness while transmitting the other. This phenomenon could be applied to the design of broadband circular polarizers or

for colour modulation. In the first case, Gansel *et al*. proposed a photonic metamaterial consisting of chiral plasmonic Au helices with mid-infrared absorption, arranged on a two-dimensional square lattice as a compact broadband circular polarizer.[67] Tuning the number of helix pitches they demonstrated experimentally that the transmittance of circularly polarized light with the same handedness was very low (below 5%) in a broad band range (from 3.75 to 7.5 µm, see Figure 7B). In the latter case, Lee *et al*. reported the use of chiral helicoid NPs with high anisotropy factor for circular polarization-dependent transmitted colours under cross-polarized conditions.[46] Figure 7C shows the polarization-resolved colours of light transmitted through dispersions of helicoid chiral particles with LSPR peaks ranging from 552 nm to 668 nm, at different rotational angles between crossed polarizers. Interestingly, the colour transformation of the different colloids was continuous and asymmetric with angle, thereby covering a wide colour range.

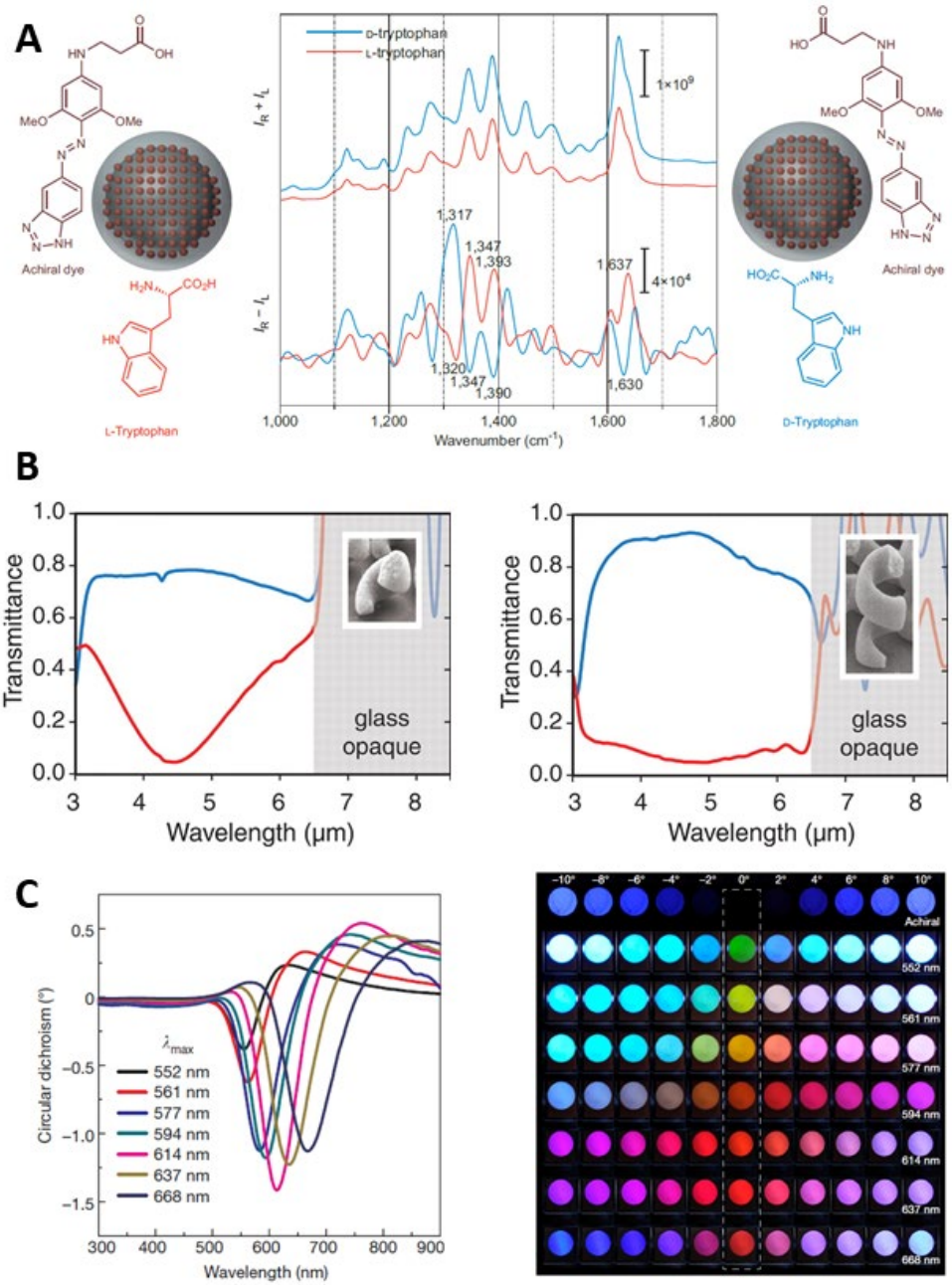

Figure 7. (A) Chirality transfer from a chiral analyte to an achiral reporter. The SERRS spectra (top) of D- and L-tryptophan bound to benzotriazole-functionalized nanotags are identical — as expected for two enantiomeric systems. Surface-enhanced Raman optical activity (SERROA) spectra (bottom) for both systems show strong chiroptical responses that are attributed to the achiral dye. I_R and I_L are the intensities of right and left polarized light, respectively. Reproduced with permission from ref. [68]. Copyright 2015 Nature publishing group. (B) Transmittance spectra measured through a photonic metamaterial composed by a 2D square lattice of slightly less than one pitch of left-handed helices (*left*) and two pitches of left-handed helices (*right*). Red and blue spectra correspond to the illumination with right- and left-handed circular polarization, respectively. Reproduced

with permission from ref. [67]. Copyright 2009 American Association for the Advancement of Science (AAAS). (C) (*Left*) CD spectra of Au helicoid NPs for different values of λ_{max} (the wavelength of maximum g-factor) and (*Right*) polarization-resolved colours of light transmitted through seven different Au helicoid NPs dispersions with different λ_{max} values (shown in the corresponding CD spectra) and an achiral nanoparticle solution (top row). Reproduced with permission from ref [46]. Copyright 2018 Nature publishing group.

Conclusions and outlook

The different examples discussed above make foreseen those wet-chemical approaches have a great potential in the synthesis of discrete metal nanoparticles with Plasmonic chirality with tight control in their shape, size and optical response. Notwithstanding, much remains to be accomplished in this field encompassing from the synthesis to the theoretical models and applications. In the following, we highlight several research directions that are particularly important to fulfil in a near future.

The positioning of chiral molecules close to, in contact or embedded in a achiral Plasmonic nanoparticle lead to a plasmon-induced chirality and CD response at the LSPR wavelengths, typically visible and NIR frequencies. Therefore, a more comprehensive theoretical understanding to correlate the positioning and orientation of the molecules on the nanoparticle, as well as to select or define the appropriate chiral molecules is crucial. Additionally, other parameters such as refractive index rather than an absorption-mediated chiral origin could be responsible of the chiroptical response in the plasmonic regime.

Regarding the synthesis of 3D chiral nanoparticles, the control over their shape and size is crucial to be able to tune the chiroptical response. Furthermore, understanding the origin of chirality in such colloidal particles is essential to further explore new synthesis approaches. For instance, the relationship/dependence between the extinction spectrum and the chiroptical properties need to study in depth. Additionally, expanding the synthesis approaches to other Plasmonic metal such as silver or copper is needed.

Another topic that could deserve more attention is the directed assembly of chiral plasmonic nanoparticles and the implications of this process in giving rise to new chiral responses based on plasmon coupling. Additionally, the development of stimuli-

responsive self-assembly of NPs with plasmonic chirality is another issue that deserves attention.[69] In that senses, DNA nanotechnology or other stimuli-responsive self-assembly approaches are expected to be applied to synthesize chiral Plasmonic nanostructures with well-defined structural morphologies with potential applicability in sensing, catalysis or storing information.

With the development of new synthetic approaches and also new morphologies the synthesis of discrete chiral nanoparticles with plasmonic chirality with high stability and monodispersity can be considered a promising tool in many applications related to chirality, such as chiral optical devices, enantioselective catalysis, chiral selective sensor and chirality separation filters among others

References

1 S. M. Douglas, H. Dietz, T. Liedl, B. Hogberg, F. Graf and W. M. Shih, *Nature*, 2009, **459**, 414-418.

2 J. Kumar, H. Erana, E. Lopez-Martinez, N. Claes, V. F. Martin, D. M. Solis, S. Bals, A. L. Cortajarena, J. Castilla and L. M. Liz-Marzan, *P Natl Acad Sci USA*, 2018, **115**, 3225-3230.

3 A. Guerrero-Martinez, B. Auguie, J. L. Alonso-Gomez, Z. Dzolic, S. Gomez-Grana, M. Zinic, M. M. Cid and L. M. Liz-Marzan, *Angew Chem Int Edit*, 2011, **50**, 5499-5503.

4 X. L. Wu, C. L. Hao, J. Kumar, H. Kuang, N. A. Kotov, L. M. Liz-Marzan and C. L. Xu, *Chem Soc Rev*, 2018, **47**, 4677-4696.

5 M. Hentschel, M. Schaferling, X. Y. Duan, H. Giessen and N. Liu, *Sci Adv*, 2017, **3**.

6 A. G. Mark, J. G. Gibbs, T. C. Lee and P. Fischer, *Nat Mater*, 2013, **12**, 802-807.

7 A. Kuzyk, R. Schreiber, Z. Y. Fan, G. Pardatscher, E. M. Roller, A. Hogele, F. C. Simmel, A. O. Govorov and T. Liedl, *Nature*, 2012, **483**, 311-314.

8 B. Han, Z. N. Zhu, Z. T. Li, W. Zhang and Z. Y. Tang, *J Am Chem Soc*, 2014, **136**, 16104-16107.

9 J. Kumar, K. G. Thomas and L. M. Liz-Marzan, *Chem Commun (Camb)*, 2016, **52**, 12555-12569.

10 A. Cecconello, L. V. Besteiro, A. O. Govorov and I. Willner, *Nat Rev Mater*, 2017, **2**.

11 M. J. Urban, C. Q. Shen, X. T. Kong, C. G. Zhu, A. O. Govorov, Q. B. Wang, M. Hentschel and N. Liu, *Annu Rev Phys Chem*, 2019, **70**, 275-299.

12 W. Ma, L. G. Xu, A. F. de Moura, X. L. Wu, H. Kuang, C. L. Xu and N. A. Kotov, *Chem Rev*, 2017, **117**, 8041-8093.

13 C. Zhou, X. Y. Duan and N. Liu, *Accounts Chem Res*, 2017, **50**, 2906-2914.

14 D. M. Solis, J. M. Taboada, F. Obelleiro, L. M. Liz-Marzan and F. J. G. de Abajo, *Acs Nano*, 2014, **8**, 7559-7570.

15 R. W. Yu, L. M. Liz-Marzan and F. J. G. de Abajo, *Chem Soc Rev*, 2017, **46**, 6710-6724.

16 V. Myroshnychenko, J. Rodriguez-Fernandez, I. Pastoriza-Santos, A. M. Funston, C. Novo, P. Mulvaney, L. M. Liz-Marzan and F. J. G. de Abajo, *Chem Soc Rev*, 2008, **37**, 1792-1805.

17 X. T. Kong, L. V. Besteiro, Z. Wang and A. O. Govorov, *Adv Mater*, 2018, e1801790.

18 A. O. Govorov, Z. Y. Fan, P. Hernandez, J. M. Slocik and R. R. Naik, *Nano Lett*, 2010, **10**, 1374-1382.
19 A. O. Govorov, *J Phys Chem C*, 2011, **115**, 7914-7923.
20 Z. Y. Fan and A. O. Govorov, *Nano Lett*, 2012, **12**, 3283-3289.
21 A. Ben-Moshe, B. Maoz, A. O. Govorov and G. Markovich, *Chem Soc Rev*, 2013, **42**, 7028-7041.
22 B. M. Maoz, Y. Chaikin, A. B. Tesler, O. Bar Elli, Z. Y. Fan, A. O. Govorov and G. Markovich, *Nano Lett*, 2013, **13**, 1203-1209.
23 H. Zhang and A. O. Govorov, *Phys Rev B*, 2013, **87**.
24 A. Guerrero-Martinez, J. L. Alonso-Gomez, B. Auguie, M. M. Cid and L. M. Liz-Marzan, *Nano Today*, 2011, **6**, 381-400.
25 L. M. Kneer, E. M. Roller, L. V. Besteiro, R. Schreiber, A. O. Govorov and T. Liedl, *Acs Nano*, 2018, **12**, 9110-9115.
26 Z. N. Zhu, W. J. Liu, Z. T. Li, B. Han, Y. L. Zhou, Y. Gao and Z. Y. Tang, *Acs Nano*, 2012, **6**, 2326-2332.
27 B. Auguie, J. L. Alonso-Gomez, A. Guerrero-Martinez and L. M. Liz-Marzan, *J Phys Chem Lett*, 2011, **2**, 846-851.
28 J. T. Collins, C. Kuppe, D. C. Hooper, C. Sibilia, M. Centini and V. K. Valev, *Adv Opt Mater*, 2017, **5**.
29 M. L. Nesterov, X. H. Yin, M. Schaferling, H. Giessen and T. Weiss, *Acs Photonics*, 2016, **3**, 578-583.
30 A. O. Govorov and Z. Y. Fan, *Chemphyschem*, 2012, **13**, 2551-2560.
31 V. V. Klimov, I. V. Zabkov, A. A. Pavlov and D. V. Guzatov, *Opt Express*, 2014, **22**, 18564-18578.
32 X. Lan, X. X. Lu, C. Q. Shen, Y. G. Ke, W. H. Ni and Q. B. Wang, *J Am Chem Soc*, 2015, **137**, 457-462.
33 Z. Y. Fan, H. Zhang and A. O. Govorov, *J Phys Chem C*, 2013, **117**, 14770-14777.
34 B. T. Draine, *Astrophys J*, 1988, **333**, 848-872.
35 F. Hao, C. L. Nehl, J. H. Hafner and P. Nordlander, *Nano Lett*, 2007, **7**, 729-732.
36 J. Jin, *The Finite Element Method in Electromagnetics*, Wiley, New York, 2002.
37 P. P. Wang, S. J. Yu, A. O. Govorov and M. Ouyang, *Nat Commun*, 2017, **8**.
38 S. Lee, J. H. Kang, S. Yoo and Q. H. Park, *Sci Rep-Uk*, 2018, **8**.
39 W. X. Zhang, T. Wu, R. Y. Wang and X. D. Zhang, *Nanoscale*, 2017, **9**, 5701-5707.
40 G. Zheng, Z. Bao, J. Perez-Juste, R. Du, W. Liu, J. Dai, W. Zhang, L. Y. S. Lee and K. Y. Wong, *Angewandte Chemie*, 2018.
41 J. Yan, Y. D. Chen, S. Hou, J. Q. Chen, D. J. Meng, H. Zhang, H. Z. Fan, Y. L. Ji and X. C. Wu, *Nanoscale*, 2017, **9**, 11093-11102.
42 S. Hou, J. Yan, Z. J. Hu and X. C. Wu, *Chem Commun*, 2016, **52**, 2059-2062.
43 C. L. Hao, L. G. Xu, M. Z. Sun, W. Ma, H. Kuang and C. L. Xu, *Adv Funct Mater*, 2018, **28**.
44 X. L. Wu, L. G. Xu, W. Ma, L. Q. Liu, H. Kuang, W. J. Yan, L. B. Wang and C. L. Xu, *Adv Funct Mater*, 2015, **25**, 850-854.
45 C. L. Hao, L. G. Xu, W. Ma, X. L. Wu, L. B. Wang, H. Kuang and C. L. Xu, *Adv Funct Mater*, 2015, **25**, 5816-5822.
46 H. E. Lee, H. Y. Ahn, J. Mun, Y. Y. Lee, M. Kim, N. H. Cho, K. Chang, W. S. Kim, J. Rho and K. T. Nam, *Nature*, 2018, **556**, 360-+.
47 S. Ostovar pour, L. Rocks, K. Faulds, D. Graham, V. Parchaňský, P. Bouř and E. W. Blanch, *Nat Chem*, 2015, **7**, 591-596.
48 N. H. Cho, G. H. Byun, Y. C. Lim, S. W. Im, H. Kim, H. E. Lee, H. Y. Ahn and K. T. Nam, *Acs Nano*, 2020, **14**, 3595-3602.
49 H. E. Lee, R. M. Kim, H. Y. Ahn, Y. Y. Lee, G. H. Byun, S. W. Im, J. Mun, J. Rho and K. T. Nam, *Nat Commun*, 2020, **11**.

50 G. Gonzalez-Rubio, J. Mosquera, V. Kumar, A. Pedrazo-Tardajos, P. Llombart, D. M. Solis, I. Lobato, E. G. Noya, A. Guerrero-Martinez, J. M. Taboada, F. Obelleiro, L. G. MacDowell, S. Bals and L. M. Liz-Marzan, *Science*, 2020, **368**, 1472-+.
51 M. Nakagawa and T. Kawai, *J Am Chem Soc*, 2018, **140**, 4991-4994.
52 A. Ben-Moshe, S. G. Wolf, M. Bar Sadan, L. Houben, Z. Y. Fan, A. O. Govorov and G. Markovich, *Nat Commun*, 2014, **5**.
53 K. Saito and T. Tatsuma, *Nano Lett*, 2018, **18**, 3209-3212.
54 K. Morisawa, T. Ishida and T. Tatsuma, *Acs Nano*, 2020, **14**, 3603-3609.
55 B. Sepulveda, P. C. Angelome, L. M. Lechuga and L. M. Liz-Marzan, *Nano Today*, 2009, **4**, 244-251.
56 K. M. Mayer and J. H. Hafner, *Chem Rev*, 2011, **111**, 3828-3857.
57 H. H. Jeong, A. G. Mark, M. Alarcon-Correa, I. Kim, P. Oswald, T. C. Lee and P. Fischer, *Nat Commun*, 2016, **7**.
58 W. J. Liu, Z. N. Zhu, K. Deng, Z. T. Li, Y. L. Zhou, H. B. Qu, Y. Gao, S. N. Che and Z. Y. Tang, *J Am Chem Soc*, 2013, **135**, 9659-9664.
59 M. L. Brongersma, N. J. Halas and P. Nordlander, *Nat Nanotechnol*, 2015, **10**, 25-34.
60 Y. R. Fang, R. Verre, L. Shao, P. Nordlander and M. Kall, *Nano Lett*, 2016, **16**, 5183-5190.
61 P. Herves, M. Perez-Lorenzo, L. M. Liz-Marzan, J. Dzubiella, Y. Lu and M. Ballauff, *Chem Soc Rev*, 2012, **41**, 5577-5587.
62 G. V. Hartland, *Chem Rev*, 2011, **111**, 3858-3887.
63 F. L. Gao, M. Z. Sun, W. Ma, X. L. Wu, L. Q. Liu, H. Kuang and C. L. Xu, *Adv Mater*, 2017, **29**.
64 M. Kim, J. H. Lee and J. M. Nam, *Adv Sci*, 2019, **6**.
65 A. R. Miandashti, L. K. Khorashad, M. E. Kordesch, A. O. Govorov and H. H. Richardson, *Acs Nano*, 2020, **14**, 4188-4195.
66 I. Dolamic, B. Varnholt and T. Burgi, *Nat Commun*, 2015, **6**.
67 J. K. Gansel, M. Thiel, M. S. Rill, M. Decker, K. Bade, V. Saile, G. von Freymann, S. Linden and M. Wegener, *Science*, 2009, **325**, 1513-1515.
68 V. Mujica, *Nat Chem*, 2015, **7**, 543-544.
69 M. Grzelczak, L. M. Liz-Marzan and R. Klajn, *Chem Soc Rev*, 2019, **48**, 1342-1361.